Laser induced electron bursts for the diagnostic of Hall thruster plasma

IEPC-2007-139X-C5G2B5D2F1

Presented at the 30th International Electric Propulsion Conference, Florence, Italy
September 17-20, 2007

T. Gibert* A. Leufroy† A. Bouchoule ‡
Groupe de Recherches sur l'Energétique des Milieux Ionisés, Orléans, 45000, France

A. Lazurenko§
Thales Electron Devices GmbH, Ulm, D-89077, Germany

The present development of Hall thrusters for satellite control and space mission technologies represent a new step towards their routine use in place of conventional thermal thrusters. In spite of their long R and D history, the complex physics of the E $\times$ B discharge at work in these structures has prevented, up to now, the availability of predictive simulations. The electron transport in the accelerating layers of these thrusters is one of the remaining challenges in this direction. From the experimental point of view, any diagnostics of electron transport and electric field in this critical layer would be welcome for comparison with code predictions. Appropriate diagnostics are difficult, due to the very aggressive local plasma conditions. This paper presents the second step in the development of a new tool for characterization of the plasma electric field in the very near exhaust thruster plume. The main idea is to use very short bursts of electrons, probing local electron dynamics in this critical plume area. Such bursts can be obtained through photoelectric emission induced by a UV pulsed laser beam on a convenient target. The previous step of the development of this tool is recalled shortly in the first part part of the paper; an experimental set-up, devoted to follow electron cloud dynamic in vacuum at the exit plan of thruster is presented in the second part; the last part presents the set-up for characterizing the transport of injected bursts in the very near exhaust thruster plume wich was available in the PIVOINE facility. Theses experiments require a preliminary evaluation of electron trajectories which was achieved by using simulation code. Simulation implementation is presented in the second part. paper, The same electron burst injection could also be a valuable input in the present discussion on the physics of the 5-10 MHz instability observed in almost all Hall thrusters.

(Some figures in this article are in colour only in the electronic version).

Nomenclature

ε_0	Permittivity of free space
λ	Radiation wavelength
μ	Electron mobility
c	Light velocity
dt	Time step
i, j	Particles indexes
h	Planck constant
m	Electron mass
q	Electron charge

*Doctor, Propulsion, titaina.gibert@univ-orleans.fr.
†Ph.D. student, Propulsion, alain.leufroy@univ-orleans.fr.
‡professor, a.bouchoule@wanadoo.fr
§Doctor, Business Development, Alexey.Lazurenko@thalesgroup.com.

I. Introduction

This paper presents the second step of development of a new diagnostic tool for Hall effect thruster plasma.The basic idea is to use short electron bursts as test particules in order to characterize the electron dynamics in the exit area of the thruster channel.

The first aim of such diagnostic was to verify more precisely assumptions about the nature of high frequency instabilities observed in this region, by comparing dynamic of injected electrons with instantaneous fluctuations[1]. For a precise comparison, electron bursts are produced with same temporal characteristic as the peaks recorded for spontaneous fluctuations on antenna signals, i.e. with few nanoseconds time duration.

The second aim was to use such bursts as diagnostic for values of the electric field at exit of channel, by measurement of their azimuthal drift velocity.

The optically controlled electron burst is injected in the thruster plume plasma near the channel exit plan. Collectors and antennas, arranged in azimuthal positions around ceramics of the thruster, are used to follow its trajectories. Average value of the electric field along their trajectory is derived from the azimuthal drift velocity obtained by delays between collectors or antennae signals. Such experimental data can help in the improvement of the predictivity of hybrid codes where anomalous electron transport in this region remain dependant of adjustable Bohm-like coefficient [2].

II. Generation of electron burst

The photo electric generation of short electron bursts has already been used for various purposes. One of the most developed was the injection of ultra-short bursts in RF accelerators [3]. Such electron bursts have also been used in the eighties for diagnostics of RF plasma sheaths in $13.56\,MHz$ capacitive low pressure discharges [4–6], where the injection time within an RF period revealed the time behaviour of the RF sheaths [5–10]. The first step of the development of this tool for the diagnostic of the near exhaust plasma of a Hall thruster was presented in details elsewere [11]. This step is recalled shortly in this part. A test of azimuthal drift characterization has been achieved in vacuum conditions, by injecting bursts in the SPT 100ML magnetic field with an homogeneous axial electric field. Preliminary experiments in thruster conditions, achieved in PIVOINE facility, will be presented and discussed in the last section.

A. experimental device

The short electron burst production has been characterized for a selected laser-material system and in a wide range of operation parameters. The UV laser pulse was obtained from a quadrupled frequency output of a Quantel Brilliant Nd- YAG laser. The energy per pulse, at a wavelength of $266\,nm$, can be adjusted by an attenuator from a few micro joules up to $6.5\,mJ$. The repetition rate is $10\,Hz$ and the overall beam diameter $5\,mm$. The pulse duration is $5\,ns$. The pulse exhibits hot spots in space and time. Taking into account the UV photon energy ($4.66\,eV$) we selected tantalum as electron emitter. The choice of a refractory metal (Ta melting temperature $3290\,K$) was more or less mandatory, as this target will support a significant heat release when installed in the Hall thruster conditions. For an averaged value of working function of around $4.3\,eV$, the laser-tantalum should be able to produce photo electrons with an escaping energy $0.36\,eV$. Recording the instantaneous burst electron current requires a specific design of a wide band pass diode device. This device is presented below.

B. wide band pass diode design

Measurements of electron burst currents at a nanosecond time scale needs special care[10]. Scheme of the diode system, where the Ta plate is the cathode, is presented in Fig. 1. This system was installed in a vacuum chamber at GREMI laboratory which is equipped with an optical and electrical feedthrough allowing transfers of the laser pulse, the electron current signal and Ta cathode dc polarization up to.

Recorded diode voltage signal corresponds to a current through $20\,\Omega$ in parallel with $50\,\Omega$ load ($R_{eq} = 14\,\Omega$). The derivation of the total burst charge Q and electron number N_{et} from the recorded diode signal. The collected charge Q is calculated with Eq. 1.

$$Q = \int I(t) \cdot dt = \int \frac{V(t)}{R_{eq}} \cdot dt \tag{1}$$

The effective efficiency η_{eff} of the photoelectric process is defined as the ratio of the number of photo electronsN_{et} to the number N_{ph} of UV photons impinging the Ta cathode. η_{eff} calculation is given in Eq. 2.

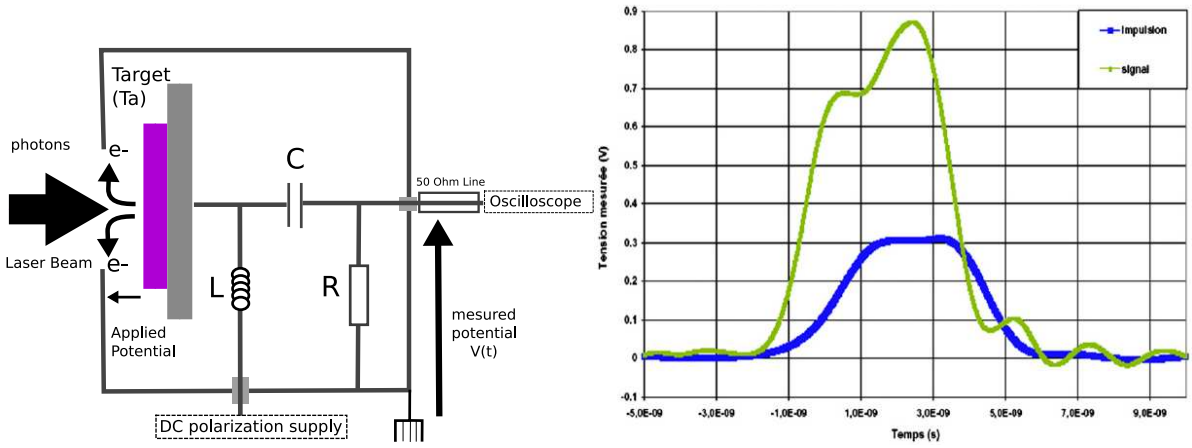

(a) Vacuum diode set-up

(b) Example of the photodiode PIN signal and diode current. Excitation pulse (blue line) and the target signal (green line)

[h]

Figure 1. Vacuum diode set-up and typical measure of transient photo electronic current. $R = 20\Omega$, $C = 13\,pF$

$$\eta_{eff} = \frac{N_{eq}}{N_{ph}} = \frac{1}{N_{ph}}\frac{Q}{q} = \frac{hc}{qE_{laser}\lambda}\int\frac{V(t)}{R_{eq}}\cdot dt \tag{2}$$

This effective efficiency is not the quantum efficiency η_{eq} defined as the ratio of the number of emitted photo electrons leaving the Ta plate N_{eq} to the number of UV photons N_{ph} (see Eq. 3).

$$\eta_{eq} = \frac{N_{eq}}{N_{ph}} \tag{3}$$

Space charge effects, as evidenced in other studies[4–6], can induce backward trajectories of emitted electrons towards the emitter surface and a collection efficiency is defined in Eq. 4 and Eq. 5:

$$\eta_{coll} = \frac{\eta_{eff}}{\eta_{eq}} = \frac{N_{et}}{N_{eq}} \tag{4}$$

$$\eta_{eff} = \eta_{eq}\cdot\eta_{coll} \tag{5}$$

C. Extraction of electrons from Ta

Diode voltage and laser pulse energy was varied. The collection efficiency should increase when the diode voltage increases and when the laser pulse energy decreases, as both variations lead to a reduction of the space charge effects.

Recordings of the laser pulse shape of the electron current pulses allows to establish optimal conditions for space charge effect reduction (Fig. 2).

As shown in Fig. 2, for laser energy less than $0,12\,mJ$ and applied potential on collector over than $200V$ the collection efficiency is equal to 1. Electrons quantification during one laser shot were obtained by measuring electronic current. Then quantum efficiency of tantalum were deducted at the wavelength of $266nm$:

$$\eta_{eq} = 1.5\cdot 10^{-6} \tag{6}$$

Otherwise, space charge effect affects trajectories of electrons so damage the signal. A specific 1-D Particle-In-Cell code is implemented in order simulate the space charge effect. The results of this first approximation, given in Fig.s 3a and 3b, show a rather good agreement with experimental data.

The implantation of this set-up at the exit channel of the SPT-100-ML, built in PIVOINE facility at ICARE laboratory in Orleans, has clearly shown the injection of electron into the plasma. The second part of this paper presents additional investigations which consists in following the electron cloud and implementing a simulation code of trajectories of electrons.

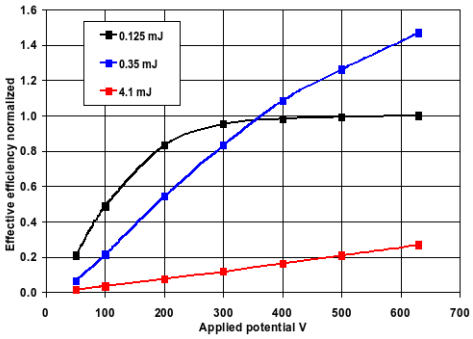

Figure 2. Collection efficiency.

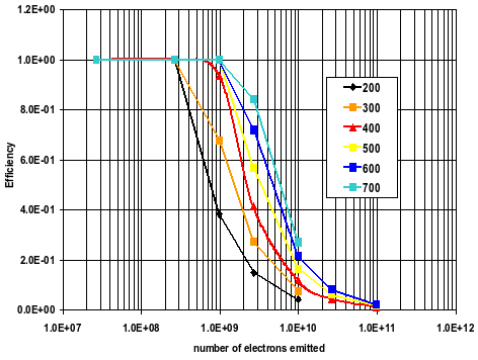

(a) Normalized effective efficiency as function of number of total emitted electrons

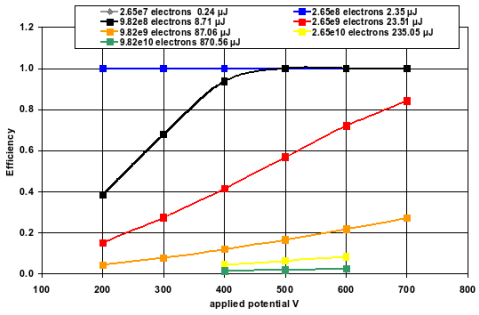

(b) Normalized effective efficiency as function of applied potential

Figure 3. Simulation results of space charge effect by 1-D PIC code

III. Electron burst dynamics in SPT 100ML magnetic field and homogeneousaxial electric field

A. 3-D Particle In Cell Simulation

The first part of this study concerned a simulation of electron trajectoriesin these vacuum conditions.

The stationary magnetic field this Hall thruster has a trap-like configuration for electrons (see e.g. [12]). Numerous investigations showed that the electron current magnetic field can be neglected [13,14]. A condition on electron initial velocity, allowing magnetic reflexion near the central pole of the magnetic field, is derived from the conservation of the magnetic moment :

$$\mu = \frac{m \cdot v_{\perp}^2}{2B} = const \tag{7}$$

where m is the electron mass, $v_{\perp}^2$ is its velocity perpendicular to the magnetic field B. The electron can perform a bounce motion between the mirror points if its velocity is chosen in such a way as not to collide with the thruster body. This adiabatic invariant (Eq. 7) is not violated by the magnetic field gradients: their typical scale is 10 mm, whereas the electron Larmor radius $r_L = 0.75\,mm$ for 10 eV and $B = 10\,mT$. When an axial, homogeneous, electric field is applied injected electrons drift in azimuthal direction with the velocity:

$$v_{drift} = \frac{E \times B}{B^2} \tag{8}$$

is typically of the order of $\sim 10^6\,m.s^{-1}$ in the plasma of Hall thrusters near channel exit. The aim of this simulation is to define initial electron velocities leading to magnetic reflexion and allowing observation of the azimuthal drift across the channel exit.

1. *Simulation model*

Mathematical modeling and numerical simulation of electrons trajectories that are plasma components with consideration of space charge effects are of great importance in order to understand electron mobility in the plasma of hall thrusters.

The distribution of particles in phase space of coordinates and velocities is describes by the distribution function. In consideration of particles space effects and external fields that take place in the output plan of hall thrusters, the motion of electrons could be described in a general dynamic equation which results of a simplified Vlasov equation (Eq. 9).

$$\frac{d}{dt}(\vec{v}) = \frac{q}{m}\left(\vec{E}_{spt} + \vec{E}_{cheff} + \vec{v} \times \vec{B}\right) \tag{9}$$

Finite particle methods are the most powerful methods for the numerical simulation of plasma dynamics and motion of charged particles as electrons are. These methods allow studying the detailed characteristics of continuous medium, taking into account the distribution functions of particles (spatial, and velocity distributions), real self and external fields, particle-particle interactions and many other effects.

Within plasma physics, Particle In Cell (PIC) simulation has been used successfully to study electron acceleration. The PIC method refers to a technique used to solve a certain class of partial differential equations as our motion equation - due to the local charge effect which depends on particles distribution. Individual particles in a Lagrangian frame are tracked in continuous phase space, by solving motion equation at every integration step, whereas other external fields are computed on Eulerian (stationary) mesh points.

We use the P^3M mode of PIC which includes particle-mesh and particle-particle interactions.

2. *Simulated equations*

Because Eq. 10 cannot be solved directly, we have to adapt it according as possible to the PIC method.

Firstly, PIC method allow us to discretize time line. By this way the differential expression can be computed as a ratio of finite differences.

$$\frac{d}{dt}(\vec{v}) = \frac{\Delta\vec{v}}{\Delta t} = \frac{\vec{v}^{t+dt} - \vec{v}^{t}}{dt} \tag{10}$$

Secondly, space is discretized too and field values have not to be known everywhere at space consideration. These values is just been known at mesh points. $\vec{E}_{spt}$ and $\vec{B}$ became $\vec{E}_{spt}(x,y,z)$ and $\vec{B}(x,y,z)$ at time t when the electron position is determined by the triplet (x,y,z) in the Cartesian coordinate. t is not put as an argument because electric and magnetic field are stationary.

Field values are obtained by hybrid model simulation of hall thruster plasma[2,15]. These values are given in 2-D polar coordinate maps with azimuthal symmetry.

Because of the 3-D computing particularities, charge effect is not implemented in the mesh grid as a modification of local electric field (as PIC considerations). Charge effect is described by the electric field (Eq. 11)

$$\vec{E}_{cheff} = \frac{q}{4\pi\varepsilon_0} \cdot \sum_{i\neq j}^{N} \left(\frac{\vec{ji}}{\left\| \vec{ji} \right\|^3} \right) \tag{11}$$

where N is particles number and $\vec{ji}$ is the location of the i^{th} particle.

In all these considerations Eq. 9 can be computed with Eq. 12 for a particle i.

$$\vec{v}_i^{\,t} = A \cdot \left[\vec{E}_{spt} + \vec{v}_i^{\,t} \times \vec{B} + K \cdot \sum_{i\neq j}^{N} \left(\frac{\vec{ji}}{\left\| \vec{ji} \right\|^3} \right) \right] + \vec{v}_i(t) \tag{12}$$

where A is $\frac{q}{m}$ and K is $\frac{q}{4\pi\varepsilon_0}$.

3. *Approximations*

PIC method is susceptible to error from so-called discrete particle noise. This error are statistical in nature [16].

Error effects can be explain approximately (Eq. 13) by looking for energy conservation with no electric field and charge effect. In this approximation $\overrightarrow{B} = B_z\overrightarrow{e_z}$ and $\overrightarrow{v} = v_x\overrightarrow{e_x} + v_y\overrightarrow{e_y}$.

$$v^{t+dt} = \sqrt{(v_x^{t2} + v_y^{t2})(B_z^2.dt^2 + 1)} \tag{13}$$

Error depends on time discretization with dt^2 and space discretization in B_z^2 (see Eq. 13). In theory, error is equal to zero when time and/or space steps are equal to zero.

In computing, effects of theses errors can be reduced by a nice choice of time and space steps with an acceptable execution time. These values are chose by successively decrease space and time steps discretization, till results become independent of the size of the grid mesh. By this way time step is equal to 5×10^{-15} second and space step is equal to 1×10^{-4} meter.

4. *Results*

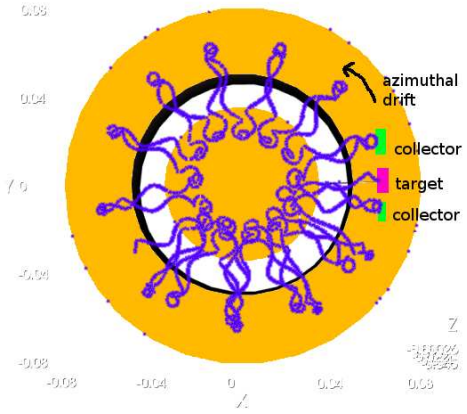

Figure 4. Theoretical electron trajectory.

The Fig. 4 show a theoretical electron trajectory. As expected magnetic mirror effects at high value of the magnetic field. However, the magnetic value B_{mirror} of the mirror effect is given by :

$$\frac{v_{\|0}^2}{v_{\|0}^2 + v_{\perp 0}^2} = \frac{B_{init}}{B_{mirror}}$$

where B_{init} is the initial magnetic field value, $v_{\|0}$ and $v_{\perp 0}$ are the initial velocity parallel and perpendicular to $\overrightarrow{B_{init}}$. The value of B_{mirror} depends on initial conditions. Therefore the turning back point could be placed on the thruster where electron will be lost.

The next aim is to build an experimental set up in order to verify simulation code on a simple configuration by injecting electron in vacuum without plasma at exit channel of an SPT 100ML.

B. Experimental results

1. *Experimental conditions*

In this experiment, an homogeneous axial electric field is applied between two parallel aluminium plates as shown in Fig. 5b. The goal was to demonstrate in this simple situation the possibility of follow the drift of electron burst.

The experiments was performed in vacuum chamber at GREMI laboratory. The vacuum chamber is a stainless steel cylinder of length $1\,m$, diameter $0.5\,m$ and volume $0.196\,m^3$. Three turbo-molecular pumps (Varian Turbo V1800A, TV551 Navigator and Adixen ATH 2300M) allow a working pressure of $10^{-6}\,Torr$.

The overall experimental scheme is shown in Fig. 5.

The magnetic field (Fig. 5a) varied with the thruster magnetic coil current tuned from $3A$ to $6A$. The SPT 100ML magnetic system is far from saturation in this range and magnetization currents in the internal and external coils were varied synchronously. Therefore the magnetic field topology was unchanged.

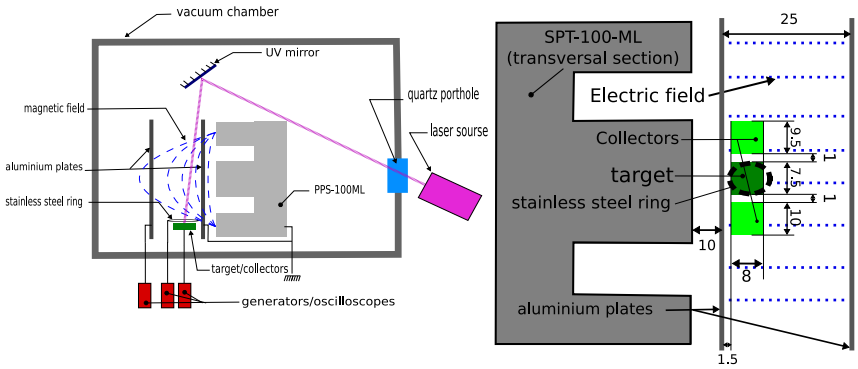

(a) global view

(b) side view (measured distance within millimeters)

Figure 5. Experimental set-up for the vacuum electron injection.

The electric field, produced by two aluminum plates distant of 25 mm (Fig. 5b). The upstream plate was always kept at ground potential; the positive dc potential was applied to the downstream plate. The biasing potential between aluminium plates was varied from 100 V to 300 V, which corresponds to the electric fields of from 40 to $120 V \cdot cm^{-1}$ of the order of electric field in Hall thruster [12,17–19].

The electron bursts are created as describe previously : the same quadrupled frequency Nd-YAG laser from Brilliant Quantel Company as before was utilized on the same Ta plate. The laser was adjusted to the wavelength of λ = 266 nm

The electron extraction of electrons is obtained with a stainless steel ring, placed at $0,5\,cm$ in front of the Ta plate, and polarised positively at *extraction potential* to extract photo electrons.

The electron detection of electron bursts is provided by two plates made in non-magnetic stainless steel. These plates are placed on each side of the Ta plate and were connected via coaxial $50\,\Omega$ cables of the same length ($\sim 2.5m$) to the digital Tektronix oscilloscope TDS3054 AC - $50\,\Omega$input.

The electromagnetic noise due to laser electronics is comparable with the collector signal during several hundreds of ns after injection (Fig. 6b). This noise was recorded by blocking the laser beam. Then subtracted to the signal recorded with laser beam on. This subtracting method revealed the signal related to photo electron bursts (Fig. 8).

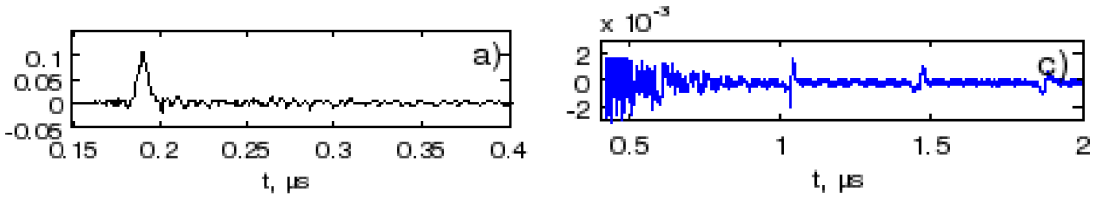

(a) Typical target signal (V)

(b) Typical collector signal (V)

Figure 6. Electron injection into the vacuum electric and magnetic fields (averaged over 64 acquisitions) for high magnetic field ($I_b = 6A$).

2. *Results*

At the working pressure $10^{-6} Torr$ the equilibrium neutral gas density is $\sim 310^{16} m^{-3}$ and the characteristic $\overline{e} - N2$ collision frequency is $610^3 s^{-3}$ for 10 eV electrons (cross-section data from [20]). Therefore, collisions have negligible effect on the electron dynamics at the time-scale of interest (several hundreds nanoseconds).

The position of target was adjusted in order to allow electron cloud rotations which depend on the mirror effect along trajectories.

The extraction potential was varied in the range of +100 ... -50 V to simulate different injection conditions. The laser pulse energy is set to 3 mJ at the output of the laser source. The extraction potential is typically set to 50 V in order to preserve electric field distribution between aluminium plates from the ring potential.

A typical photo electron is shown in Fig. 8. Zero time-line correspond to laser beam emission. The peak in the target signal is positive and the ones in collector signal are negative. The first one corresponds to emitted electrons

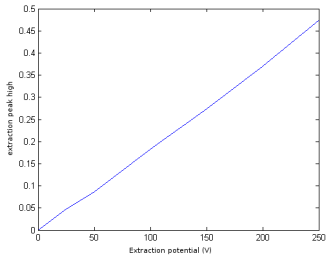

Figure 7. Target peak high as a function of extraction potential

current detection whereas latters correspond to charged particles detection. Every target signals are similar to the one presented as before.

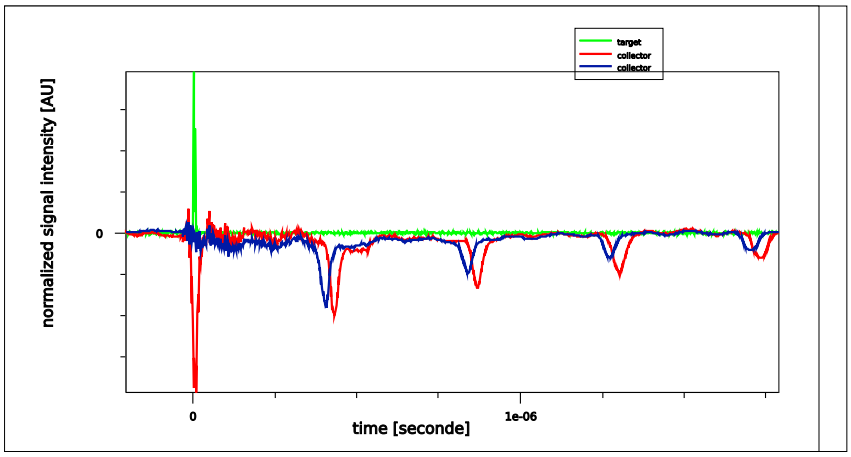

Figure 8. Typical post-processed signals.

The first peak which appears on one collector signal at few ns corresponds to one round trip of electrons between both magnetic poles of the thruster over the exit channel as expected from theoretical electrons trajectory (Fig. 4).

Every peak in the same line corresponds to each time electron cloud is detected by the corresponding collector. Because of the polarized ring, target signal cannot detect electron cloud and the signal have just one peak. The period correlates very well with the period of electron drift in crossed electric and magnetic fields. It is called the *drift period*.

The azimuthal drift was also directly evidenced by inserting a blocking ceramic barrier. Signal s with and without this barrier are shown in Fig. 9.

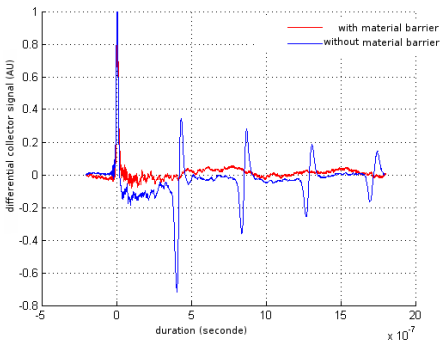

Figure 9. Effect of material barrier on the electron paths.

Another cause of electron leakage is collection of electrons by thruster structure. Electron cloud tapping is defined by mirror point positions relatively the thruster body. For small values of magnetic field, under the same

injection conditions, the mirror points are close to the thruster body and electron leakage is increased (Fig. 10).

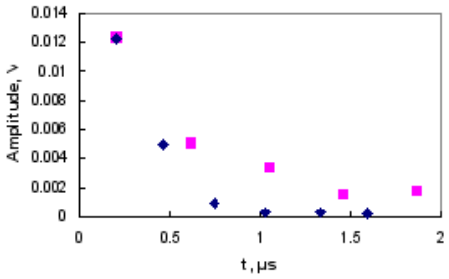

Figure 10. Collector signal amplitude at the moments of electron cloud passage in proximity. Diamonds -$I_b = 4A$, rectangles -$I_b = 6A$.

A parametric investigation of the drift period as function of magnetic and electric fields shows a good agreement with expectations (Fig. 11).

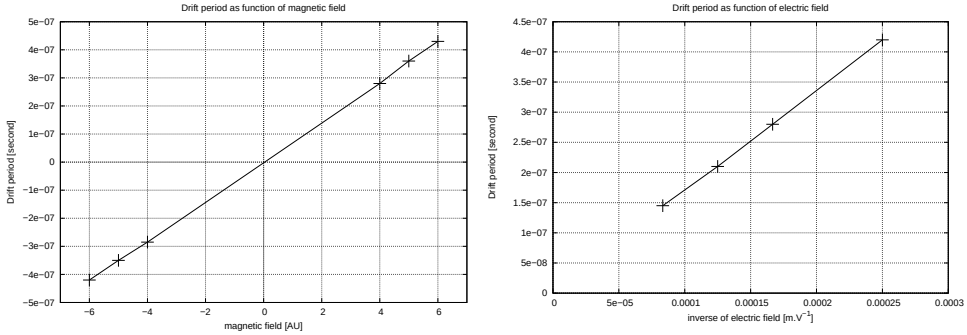

(a) Drift period as a function of magnetic field. (negative values are used to indicate that drifts are in contrary direction)

(b) Drift period as a function of electric field

Figure 11. Azimuthal drift period of electron cloud as function of magnetic and electric field.

These results show that the photo electron injection can be adjusted for trajectories magnetically reflected and the electron density is not too high. In fact electron packets can be evidenced after at least four azimuthal these vacuum conditions.

The last part of this paper presents a preliminary investigation in thruster operating conditions.

IV. Electron Injection into the thruster plasma

A. Experimental set-up

The facility test PIVOINE, operated at ICARE laboratory of CNRS in Orleans campus, is a large vacuum chamber, with a $4\,m$ length and $2.2\,m$ diameter. This facility is equipped with cryo-pumps and cryo-panels capable to ensure a working pressure of $10^{-5}\,Torr$ (on Xenon) with a rate flow of 50 mg/s of Xenon.

Laser targets are made from 8 mm x 17 mm Ta sheets bent as shown in Fig. 12. The ion plume facing part is 8 mm x 8 mm. Three Targets are installed onto an only bloc of Macor-type ceramic. Each is spaced 2 mm appart. Coaxial 50 Ω cables were screwed to the target rear parts. Two target blocs were installed around the thruster accelerating channel, 5 mm downstream, and in two radial positions(Fig. 12a) :

position *1* at $R = 61\,mm$ and at $\theta = 0^\circ$

position *2* at $R = 71\,mm$ and at $\theta = 120^\circ$

The typical external radisu of the SPT 100ML is 50 mm and an ion plume divergence angle of 45°. So at the position *1* steel plates were on the border of the plasma plume whereas at position *2* they are at outside the plume.

Each plate can operate either in electron-emitting mode or in signal-collecting mode depending on which of them is irradiated by incident laser beam.

(a) (b)

Figure 12. SPT 100ML equipped with the targets for electron injection into the plasma (targets are in the second position).

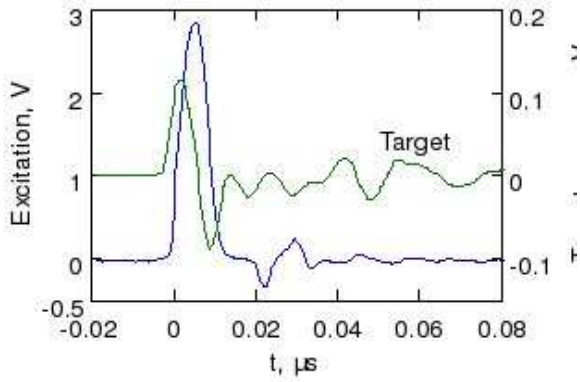

Figure 13. Target response to the excitation pulse.

The target signals were observed and recorded on digital oscilloscope Tektronix 5104B in 50 Ω acquisition mode. The whole acquisition line {target+cable} was checked against the capacitive excitation by a positive polarity pulse of several volts. A system of a photodiode coupled with an optical fiber to the laser beam is used as a synchronisation for the acquisition line. Figure 13 shows an example of circuit response. We can distinguish the signal of the photo electron from the noise.

In some of experiments inductive coils[2,21] completed the diagnostic tools (Fig. 12). They were installed outside the ionic plume around the accelerating channel. These inductive coils detect a time-varying magnetic field generated by moving charges. Therefore they would be useful in detecting injected and propagating electron charge. But during the injection the inductive coils are able to deliver only qualitative information because their passband is limited to 50 MHz whereas the involved injection time-scales lead to characteristic frequencies in excess of 200 MHz. Otherwise they are usefull to confirm the presence of electron cloud in order to confirm collectors results.

Laser source is installed outside the vacuum chamber (Fig. 14), providing the incidence angle to target of 45°. Quartz window allow the UV beam entering the PIVOINE chamber. The laser beam energy is attenuated by to 45° mirrors, the window and a diaphragm. So the incident energy per pulse on the Ta target is about 1mJ.

The laser beam is guided until the target by a system of two mirrors. The incidence on the surface is 45°. A diaphragm is used in order to reduce the laser spot on the Ta plate in order to avoid irradiation of the neighbouring plate. The quadrupler crystal temperature is tuned to adust the energy per pulse. A convenient level of signal is found when the incident energy is about 1 mJ per pulse. With the value of $1.5 \cdot 10^{-6}$ for the quantum efficiency peviously deduced (Eq. 6) this lead to $2 \cdot 10^{9}$ photo electrons and a total escaping charge of 10^{-10} Cb.

B. Plasma parameters.

Plasma features near the Ta plate have been derived by using “Langmuir Probe” characteristics for the Ta plate itself.

We mesure the value of the floating potential $V_{fl} = -0.33V$. Assuming the value of $T_e = 7\,eV$ the density of

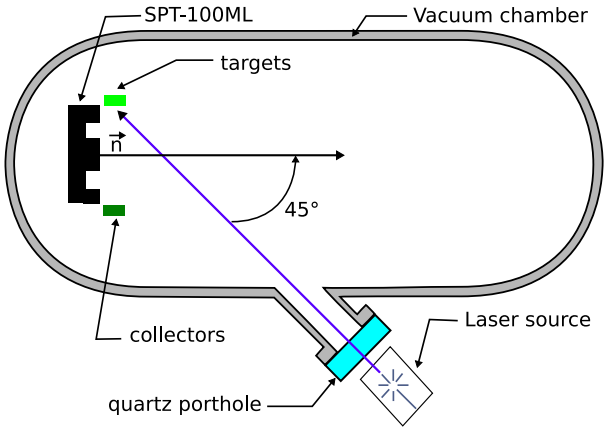

Figure 14. Optical schema of electron injection.

ions is $ni = 4 \cdot 10^{16}$. It correspond for a xenon plasma to a plasma potentiel of $5kTe$ which gives $V_p = 40\,V$.

C. Charge propagation.

The results unambiguously evidence that the electrons are really injected into the Hall thruster plasma. But their propagation in the plasma could not be confidently put in evidence.

There are indications that they penetrate at some depth into the plasma. At both target locations the electric and magnetic fields are likely to be non-parallel. The reason for this is that the equipotentials in Hall thrusters do not deviate significantly from the magnetic field lines, which is proved by numerical simulation [2]. Therefore the injected electrons, if they survive some time after the injection, will drift in these crossed fields, and the direction of this drift will depend on the magnetic field direction.

This is confirmed through inversion of magnetic filed and observation of collector signals (Fig. 15i). When magnetic field is “positive”, electrons will drift upwards to the T3 collector contributing more to its signal, and in the opposite case - to the T1 collector contributing more to its signal.

It seems that the injected electrons do not survive even one-third of the circular path in the direction of E cross B drift (between two target blocs, see Fig. 12). According to the simulation presented before, they are not likely to hit the magnetic pole. The existing strong turbulent fields, observed numerically and experimentally [22,23], could cause their dissipation. These fields could be the origine of violation of the second adiabatic invariant causing the electron cloud motion more complicated than a simple combination of mirror points bounce and drift motions. In the former experiment, we demonstrate the impact of the initial velocity orientation with respect to B on the trajectory. Namely the position of the mirror point is the key point of the trajectory. In PIVOINE set-up, the adjustement of the surface target in the fields needs about four hours and was not possible in our fixed planning. The following experiments on the diagnostic will necessitate an in-situ tuning of the plate orientation. This will constitute a further development of the diagnostic.

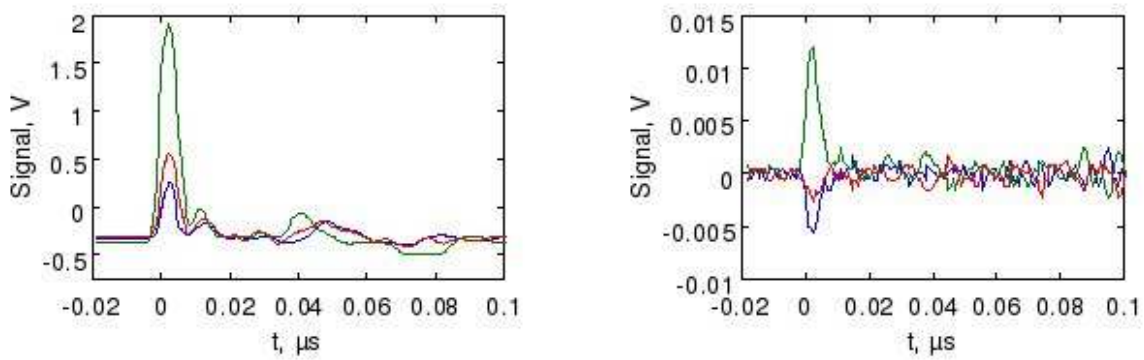

(a) Typical target signals, averaged over 128 acquisitions; T1 in blue, T2 in green, T3 in red; Laser is aimed to T2

(b) Typical target signals, averaged over 128 acquisitions; T1 in blue, T2 in green, T3 in red; Laser is aimed to T2

Figure 15. Experimental results (Part 1)

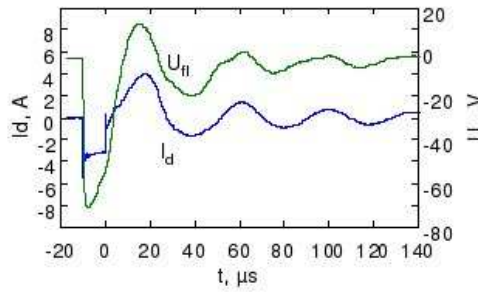

(b) Variation of I_d and T3 floating potential during and after the discharge interruption between -10μs and 0μs(average 128 acquisitions).

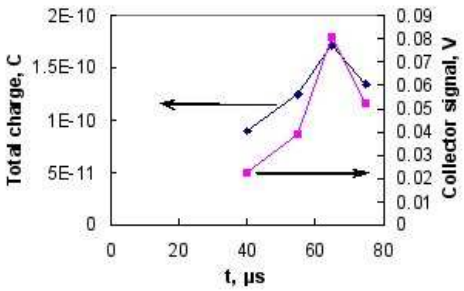

(c) Total injected charged and variation of collector amplitude (peak-peak); temporal axis correponds to that c)

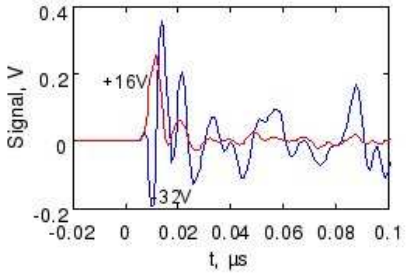

(d) Collector T1 signals with T2 biased at -32V and +16V (averaged over 128 acquisition

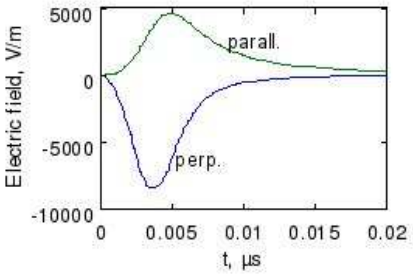

(e) Numerical simulation of the electrique field generated by the injected charge at the collector location; components parallel and perpendicular to the injection.

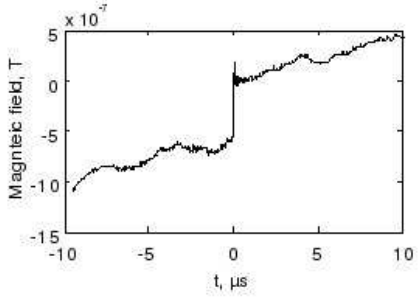

(f) Magnetic field, axial component; charge injection moment is at t=0 (averaged over 128 acquisitions).

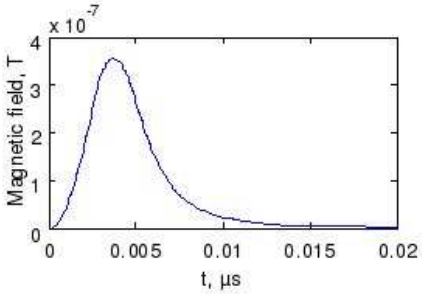

(g) Numerical simulation of the magnetic field generated by the injected chage at the collector location.

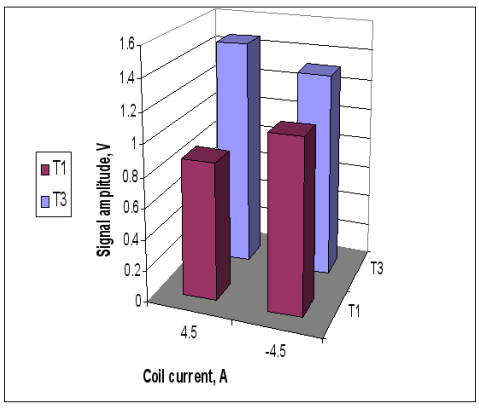

(h) Variations of collector amplitude when the direction of magnetic field is changed (averaged over 512 acquisitions).

Figure 15. Experimental results (Part 2)

V. Conclusion

This paper presents the preparative tasks of a program devoted to new diagnostics for the near exit plasma of Hall thrusters. The main aim of this program is to obtain experimental data on plasma features and especially on electron transport in this area where it is now recognized that anomalous transport phenomena dominate. Hybrid codes use an adjustable, Bohm- like, transport coefficient in this area and the calculated plasma potential map depends critically on this adjustment. By injecting low density electron bursts the program is aimed to give experimental insights on local features of the plasma electric field for comparison with code predictions.

The study of recorded signals from tantalum plate under illumination by the 4th harmonics of a Nd- YAG laser has shown that short photoelectron bursts (<7 ns), involving up to a few 10^9 electrons, can be obtained. Electrons injection in vacuum experiments has reveled that injecting conditions are important in order to get a rotate electron cloud at the exit channel of the SPT-100-ML. In this conditions the electron cloud has been followed for several turns which prove that space charge effect is not significantly important. A 3-D electron dynamics code has been implemented in order to examine the dynamics of such an electron burst experiencing the magnetic and electrostatic plasma plume distributions. Simulated results correlate electrons injection in vacuum experiments. Moreover, the burst injection in the near exit plume of a 1.5 kW class Hall thruster has been also demonstrated. Also in these conditions the plasma sheath facing the emitting Ta plate plays a significant role. However any signal of rotated electron cloud have been observed.

There are two reasons possible. The first one is that the injection conditions are not well choose. The cloud is loose before the first tour. The second reason is that anomalous transport phenomenon destroys space integrity of the electron could within the plasma. So any higher electron density can locally exist at this time-scale. It is very important to determine which one occurs in order to continue the investigation.

One way to improve these assumptions is to get precise conditions of electron injection by computing electron trajectories with datas of the SPT 100ML thruster turned on.

Acknowledgments

The authors acknowledge the technical support of J. Mathias, B.Dumax, G.Coudrat, P. Dom and the PIVOINE team: S. Sayamath, C. Legentil, and P. Lasgorceix.
This work was performed in the frame of the research group GDR number 2759 CNRS/CNES/SNECMA/Universities "Propulsion Spatiale Plasma".

References

[1]J. Kurzyna, S. Mazouffre, A. Lazurenko, L. Albarède, G. Bonhomme, K. Makowski, M. Dudeck, and Z. Peradzyński. Spectral analysis of Hall-effect thruster plasma oscillations based on the empirical mode decomposition. *Physics of Plasmas*, 12:3506–+, December 2005.

[2]G. J. M. Hagelaar, J. Bareilles, L. Garrigues, and J.-P. Boeuf. Two-dimensional model of a stationary plasma thruster. *Journal of Applied Physics*, 91:5592–5598, May 2002.

[3]R. Brogle and al. Studies of linear and nonlinear photoelectric emission for advanced accelerator applications. In *Proc. PAC Conf.*, Dallas, Tx, USA, May 1995.

[4]S. A Mitchell and R. A. Gottscho. Plasma power dissipation at wafer surfaces measured using pulsed photoluminescence spectroscopy. *J. Vac. Sci. Technol.*, A 8:1712–5, 1990.

[5]G. Selwyn and J. Singh. lasma-enhanced photoemission in argon discharge: signal characterization and silicon doping effects. *J. Vac. Sci. Technol.*, A 7:982–6, 1989.

[6]P. Davis, C. Clayton, S. Joshi C. Park S. Pellegrini C. Hairapetian, G. Hartman, and J. Rosenzweig. Quantum efficiency measurements of a copper photocathode in an rf electron gun. In *Proc. IEEE Particle Accelerator Conf.*, pages 2976–8, 1993.

[7]T. Gibert and T. Gonthiez. Resonant ionization of laser desorbed silicon. *J. Appl. Phys.*, 93:5959–65, 2003.

[8]O. D. Protopopov, E. V. Mikheeva, B. N. Shreinberg, and G. N. Shuppe. *Fiz. Tverd. Tela*, 8:1140, 1966.

[9]R. G. Wilson. *J. Appl. Phys.*, 37:3170, 1966.

[10]A. Mitchell, G. R. Scheller, and R. A. Gottscho. Photoelectron initiated avalanches in low pressure glow discharges. *Phys. Rev.*, A 40:5199Â207, 1989.

[11]L. Albarede, T. Gibert, A. Lazurenko, and A. Bouchoule. Laser injection of ultra-short electron bursts for the diagnosis of Hall thruster plasma. *Plasma Sources Science Technology*, 15:805–817, November 2006.

[12]A. I. Morozov and V. V. Savelyev. *Rev. Plasma Phys.*, 21:203, 2000.

[13]P. Y. Peterson, A. D. Gallimore, and J. M. Haas. *Phys. Plasmas, 9*, 10:4354, 2002.

[14]C. A. Thomas, N. N. Gascon, and M. A. Capelli. *Phys. Rev. E*, 74:056402, 2006.

[15]L. Garrigues, A. Heron, J. C. Adam, and J. P. Boeuf. Hybrid and particle-in-cell models of a stationary plasma thruster. *Plasma Sources Science Technology*, 9:219–226, May 2000.

[16]Hideo Okuda. Nonphysical noises and instabilities in plasma simulation due to a spatial grid. *Journal of Computational Physics*, 10:475, 1972.

[17]V. V. Zhurin, H. R. Kaufman, and R. S. Robinson. *Plasma Sources Sci. Technol.*, 8:R1, 1999.

[18]A. Bouchoule, J. P. Boeuf, A. Heron, and O. Duchemin. Physical investigations and developments of Hall plasma thrusters. *Plasma Phys. Control. Fusion*, 46 46B:407–21, 2004.

[19]L. Albarede, S. Mazouffre, A. Bouchoule, and M. Dudeck. Low frequency electron dynamics in the near field of a Hall effect thruster. *Phys. Plasmas*, 13:063505, 2006.

[20]Y. Itikawa, M. Hayashi, A. Ichimura, K. Onda, K. Sakimoto, and K. Takayanagi. *J. Phys. Chem. Ref. Data*, 15/3, 1986.

[21]C. Cavoit. Closed loop applied to magnetic measurements in the range of 0.1-50 MHz. *Review of Scientific Instruments*, 77:4703–+, June 2006.

[22]J. C. Adam, A. Heron, and G Laval. *Phys. Plasmas*, 11:295, 2004.

[23]A. Lazurenko, T. Dudok de Wit, C. Cavoit, V. Krasnoselskikh, and M. Bouchoule, A.and Dudeck. Determination of the electron anomalous mobility through measurements of turbulent magnetic field in Hall thrusters. *Phys. Plasmas*, 14:033504, 2007.